blood

2013 121: 5238-5249
Prepublished online May 10, 2013;
doi:10.1182/blood-2012-10-463414

Megakaryocytes promote murine osteoblastic HSC niche expansion and stem cell engraftment after radioablative conditioning

Timothy S. Olson, Anna Caselli, Satoru Otsuru, Ted J. Hofmann, Richard Williams, Paolo Paolucci, Massimo Dominici and Edwin M. Horwitz

Blood (print ISSN 0006-4971, online ISSN 1528-0020), is published weekly by the American Society of Hematology, 2021 L St, NW, Suite 900, Washington DC 20036.

TRANSPLANTATION

Megakaryocytes promote murine osteoblastic HSC niche expansion and stem cell engraftment after radioablative conditioning

Timothy S. Olson,[1,2] Anna Caselli,[3] Satoru Otsuru,[1] Ted J. Hofmann,[1] Richard Williams,[4] Paolo Paolucci,[3] Massimo Dominici,[3] and Edwin M. Horwitz[1]

[1]Division of Oncology and [2]Division of Hematology, Department of Pediatrics, Children's Hospital of Philadelphia, Philadelphia, PA; [3]Department of Medical and Surgical Sciences of Children & Adults, University Hospital of Modena and Reggio Emilia, Modena, Italy; and [4]Department of Oncology, St. Jude Children's Research Hospital, Memphis, TN

Key Points

- After radioablative conditioning, host megakaryocytes promote endosteal HSC niche expansion and donor stem cell engraftment.
- Thrombopoietin administration before radiation and bone marrow transplant enhances megakaryocyte promotion of HSC engraftment.

Successful hematopoietic stem cell (HSC) transplantation requires donor HSC engraftment within specialized bone marrow microenvironments known as HSC niches. We have previously reported a profound remodeling of the endosteal osteoblastic HSC niche after total body irradiation (TBI), defined as relocalization of surviving megakaryocytes to the niche site and marked expansion of endosteal osteoblasts. We now demonstrate that host megakaryocytes function critically in expansion of the endosteal niche after preparative radioablation and in the engraftment of donor HSC. We show that TBI-induced migration of megakaryocytes to the endosteal niche depends on thrombopoietin signaling through the c-MPL receptor on megakaryocytes, as well as CD41 integrin-mediated adhesion. Moreover, niche osteoblast proliferation post-TBI required megakaryocyte-secreted platelet-derived growth factor-BB. Furthermore, blockade of c-MPL–dependent megakaryocyte migration and function after TBI resulted in a significant decrease in donor HSC engraftment in primary and competitive secondary transplantation assays. Finally, we administered thrombopoietin to mice beginning 5 days before marrow radioablation and ending 24 hours before transplant to enhance megakaryocyte function post-TBI, and found that this strategy significantly enhanced donor HSC engraftment, providing a rationale for improving hematopoietic recovery and perhaps overall outcome after clinical HSC transplantation. (*Blood*. 2013;121(26):5238-5249)

Introduction

Inadequate donor hematopoietic stem cell (HSC) engraftment is a major cause of morbidity after clinical stem cell transplantation (SCT).[1] Although considerable research has focused on improving donor engraftment through refinement of the HSC graft itself,[2] therapeutic strategies to enhance receptivity of the recipient's bone marrow (BM) microenvironment are only beginning to be explored.[3]

HSCs preferentially engraft in specialized areas of BM known as HSC niches.[4] After marrow radioablation with total body irradiation (TBI), a critical site of donor HSC engraftment is the endosteal HSC niche,[5,6] located at the interface between metaphyseal trabecular bone and BM and consisting of osteoblasts, mesenchymal stromal cells, and specialized hematopoietic elements.[7,8] Recently, we reported that endosteal niche osteoblasts undergo marked expansion after TBI to form 3 or more activated layers at the endosteal surface.[9] Moreover, we discovered that TBI induces marked relocalization of megakaryocytes from the central BM space to the endosteal surface proximal to this niche osteoblast expansion.[9]

Although not previously described as endosteal niche elements, megakaryocytes are known regulators of osteoblast proliferation and differentiation.[10-13] Through expression of c-MPL and CXCR4,[14,15] megakaryocytes and HSC subpopulations share responsiveness to thrombopoietin (TPO) and stromal-derived factor (SDF)-1, both expressed by niche cells.[16] Furthermore, megakaryocytes produce mediators that directly influence homeostatic and postinjury HSC/progenitor function.[17,18] Whether megakaryocytes, which survive for several days after TBI,[19] can use these shared pathways to exert effects on the host niche post-TBI, thereby influencing donor HSC engraftment posttransplant, is unclear. Here, we show that host megakaryocytes facilitate post-TBI niche osteoblast expansion and are required for efficient donor HSC engraftment after SCT. We then demonstrate that enhancement of host megakaryocyte function before TBI promotes donor HSC engraftment and provides an effective strategy to enhance HSC engraftment after clinical transplantation.

Materials and methods

Mice and irradiation

Mouse colonies were maintained under specific pathogen-free conditions. Experiments were conducted according to protocols approved by the

Submitted October 27, 2012; accepted May 6, 2013. Prepublished online as *Blood* First Edition paper, May 10, 2013; DOI 10.1182/blood-2012-10-463414.

The online version of this article contains a data supplement.

The publication costs of this article were defrayed in part by page charge payment. Therefore, and solely to indicate this fact, this article is hereby marked "advertisement" in accordance with 18 USC section 1734.

Institutional Animal Care and Use Committee at The Children's Hospital of Philadelphia. Wild-type (WT) C57BL/6 mice were obtained from Jackson Laboratories. Homozygous c-MPL–deficient ($mpl^{-/-}$) mice on a C57BL/6 background were obtained from Genentech. H2K-green fluorescent protein (GFP) mice[20] on a C57BL6 background were obtained from institutional colonies. Mice were 6 to 12 weeks old at the start of experiments.

TBI was performed with either a ^{137}Cs source (Mark II irradiator; J.L. Sheppard and Associates) or (because of facility change) a radiograph source (X-RAD 320: Precision X-ray Inc). Radiation for osteoblast expansion and short-term (ST) primary transplantation studies was given as a single 1125 cGy dose. Secondary recipients in competitive secondary transplantation assays received 1000 to 1125 cGy in 2 split doses to decrease late nonhematologic toxicity.

Reagents and in vivo treatments

Purified blocking anti-CD41 (MWREG30) antibody (BD Biosciences) was injected (5 μg) intraperitoneally at the time of TBI and at 24 hours later. CXCR4 inhibitor AMD3100 (Sigma) was injected subcutaneously at 5 mg/kg every 12 hours post-TBI. Blocking anti-c-MPL antibody (AMM2) (generous gift of Kyowa Hakko Kirin Co.), was injected intraperitoneally (1 mg/kg) at the time of TBI. Imatinib (LC Labs) was given by gavage (300 mg/kg/dose) every 12 hours beginning the day before TBI. BrdU (BD Biosciences) was injected intraperitoneally (75 mg/kg/dose) at 24 and 42 hours post-TBI. Recombinant PDGF-BB (Peprotech) was administered at 0.5 mg/kg/dose intravenously every 12 hours post-TBI. Recombinant mouse TPO (Peprotech) was administered intraperitoneally daily at low (10 μg/kg) or high (50 μg/kg) doses.

Histology studies

Mouse femora and tibiae were fixed in 10% formalin. Bones were decalcified before dehydration, paraffin-embedded, and cut into 5- to 6-μm sections. For osteoblast proliferation analysis, sections were stained with Harris hematoxylin and eosin (Sigma-Aldrich) and were examined with 63×/1.4NA oil, 20×/0.5NA dry, and 40×/0.75NA dry objectives (Zeiss AxioImager 200M; Carl Zeiss). Photomicrographs were acquired using an Axiocam HRc camera and AxioVision 4.5SP1 software (Carl Zeiss). Individual high-power fields (HPFs) (20×) of metaphyseal bone were numerically scored in a blinded fashion from 0 to 4, representing the predominant number of contiguous endosteal cell layers. Scores for 3 to 5 HPFs per section encompassing 2 to 5 sections per mouse were averaged to generate a composite score per mouse (n ≥5 mice per group).

Megakaryocyte immunostaining was performed with polyclonal goat anti-mouse CD41 (1:50 dilution) (Santa Cruz Biotechnologies), biotinylated rabbit anti-goat secondary antibody, avidin-biotin complexes, and Novared peroxidase substrate (Vector Laboratories). Immunostained sections of metaphyseal BM were analyzed per HPF (20×) for megakaryocyte total number and location, either at the endosteal surface (within 1 cell diameter) or within the inner marrow space. At least 4 HPF per section and ≥2 sections per mouse were averaged (n ≥4 mice per group). Immunostaining for BrdU incorporation was performed with anti-BrdU-POD FAB fragments (Roche) per manufacturer protocol. Terminal deoxynucleotidyltransferase-mediated dUTP nick end labeling (TUNEL) assays were performed with a TACS 2 TdT-DAB in situ apoptosis detection kit and a TACS-Nuclease positive control (Trevigen, Inc.) per the manufacturer's instructions.

Megakaryocyte and osteoblast coculture

Primary WT megakaryocytes and osteoblasts were isolated according to previously published methods.[9,21] For coculture experiments, osteoblasts were plated onto 6-well plates (50 000 cells per well). Two days later, 1 plate was trypsinized and counted (TC10 system [BIO-RAD] or hemocytometer) to provide starting osteoblast concentration. Megakaryocytes were then plated into wells (25 000-30 000 per well) either directly onto osteoblasts or across a 0.4 μm Falcon insert (BD Biosciences). Specified cultures were treated with 5 μM of imatinib (LC Labs), 2.5 μg/mL of anti-CD41 (MWREG30), 2.5 μg/mL of anti-c-MPL (AMM2), or 2 to 10 ng/mL of recombinant PDGF-BB (Peprotech). Cocultures were incubated (37°C) for 5 days in media supplemented with 50 ng/mL of TPO. Cell growth was assessed by removing nonadherent cells, trypsinizing adherent cells, and counting cell numbers in both fractions, adjusting for percentages of $CD41^+CD45^+$ megakaryocytes and $CD41^-CD45^-$ osteoblasts, determined by flow cytometry analysis.

Primary and secondary transplantation assays

Irradiated (1125 cGy) primary recipient WT or $mpl^{-/-}$ mice ± anti-CD41 or TPO treatment received 5×10^6 whole BM cells from H2K-GFP donor mice via a tail vein injection. In primary transplant analyses, BM was collected 24 hours, 3 to 7 days, and 3 weeks post-BM transplantation (BMT). After red blood cell (RBC) lysis, BM cells were counted, stained with propidium iodide, and assessed for live GFP^+ cell percentage. Absolute GFP^+ cells were calculated as GFP^+ percentage × total BM cell count.

For secondary transplant studies, irradiated WT or $mpl^{-/-}$ primary recipients, ± anti-CD41 or TPO treatment, again received 5×10^6 GFP^+ H2K-GFP whole BM cells at 48 hours post-TBI. At 24 to 36 hours or 3 weeks post-BMT, primary recipient BM from the bilateral femora and tibiae was collected. On the basis of an established metric,[22] all BM collected from a single primary recipient was defined as a 25% BM equivalent (BME) dose. BM was pooled from ≥4 primary recipient mice per group, and a 5% or 6.25% BME dose (one fifth and one fourth of all marrow collected from a single primary recipient, respectively) was injected into irradiated WT secondary recipient mice along with 10^5 or 2×10^5 unirradiated WT whole BM cells. Secondary recipients were assessed at 3 to 28 weeks after secondary BMT for percentages of peripheral blood RBCs; platelets; $CD3^+$ T cells; $B220^+$ B cells; and $GR\text{-}1^+$ myeloid cells expressing GFP, which directly defines relative engraftment efficiency mediated by the niche in distinct primary treatment groups.

Flow cytometric measurements and enzyme-linked immunosorbent assay (ELISA)

Flow cytometry analysis was performed on BD FACSCalbur and BD FACSAria cytometers using the following antibodies (BD Biosciences): anti-mouse CD3 (154-2C11), B220 (RA3-6B2), GR-1 (RB6-8C5), CD41 (MWREG30), CD45 (30-F11), c-Kit (ACK2), SCA-1 (LY-6A/E), CD135 (A2F10), and CD127 (SB/199). Lineage (lin) staining included anti-mouse TER119, GR-1, B220, CD4 (RM4-5), CD8 (53-6.7), and CD11b (M1/70). Data were analyzed using FlowJo version 7.6.5 (Tree Star, Inc.).

To detect growth factor expression, BM cells were vigorously flushed from mouse tibiae and femora (n = 5 mice per group) and resuspended in 500 μL of phosphate-buffered saline containing 1% Nonidet-P40 (United States Biological) and protease inhibitor (Roche). Samples underwent 3 freeze-thaw cycles followed by centrifugation at 12 000 × g for 5 minutes and supernatant removal. ELISA was performed (samples run in duplicate) for IGF-1 (50 μL/assay), PDGF-BB (50 μL), vascular endothelial growth factor (VEGF) (50 μL), SDF-1 (20 μL), and TPO (30 μL) per the manufacturer's instructions (R&D systems). For pre- vs post-TBI comparisons, samples were normalized to the total BM cell number. For cell culture expression analysis, ELISA was performed on undiluted supernatants, with each independent culture (n = 3 cultures per group) run in duplicate.

Statistical analysis

Data were analyzed for statistical significance with the Student 2-tailed *t* test (Excel 2007, Microsoft Corporation) for 2-group comparisons. For multiple comparisons, nonparametric data, or binary comparisons, 1-way analysis of variance (ANOVA) (with Student-Newman-Keuls or Dunnett posttest analyses where appropriate), the Wilcoxon rank-sum test, and the Fisher exact test, respectively, were performed using Graphpad Instat v3.1 (GraphPad Software, www.graphpad.com).

Results

TBI induces active migration of megakaryocytes to the endosteal niche

At 48 hours post-TBI (1125 cGy), many megakaryocytes in WT mice relocate from the central marrow space to the endosteal

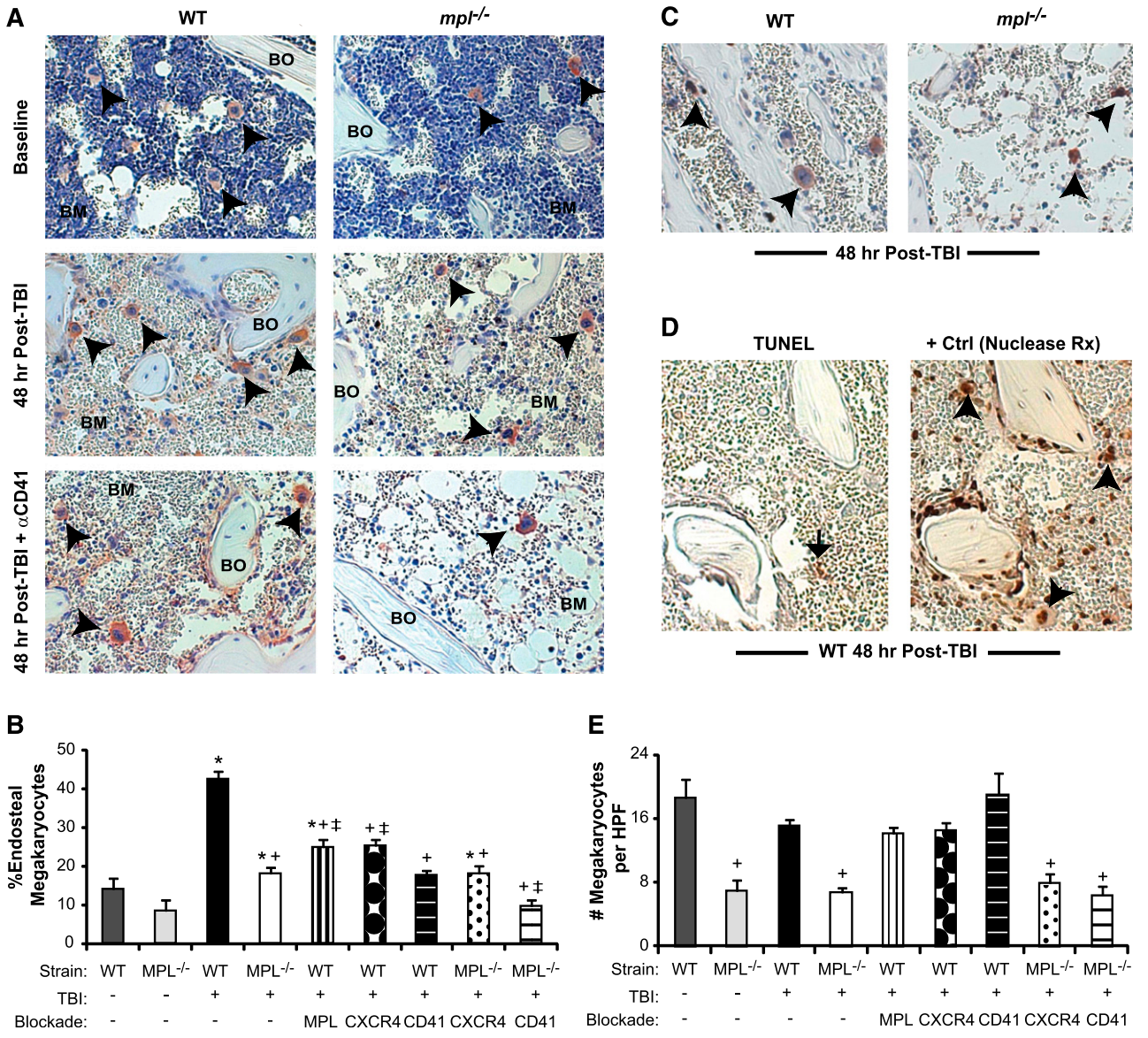

Figure 1. Megakaryocyte migration to the endosteal niche is induced by TBI and inhibited by c-MPL deficiency and CD41 blockade. (A) Immunostaining of metaphyseal bone (BO) and BM sections (20×) for CD41-expressing (red) megakaryocytes (black arrowheads) from WT (left column) and $mpl^{-/-}$ mice (right column) at baseline (top) and at 48 hours post-TBI in the presence (bottom) or absence (middle) of CD41 blockade. (B) Percentage of endosteal megakaryocytes (mean ± SEM) at baseline (no TBI) or 48 hours after TBI in WT and $mpl^{-/-}$ mice receiving TBI only, anti-c-MPL–blocking antibody (MPL), CXCR4 blockade with AMD3100 (CXCR4), or anti-CD41–blocking antibody (CD41) (n ≥4 mice per group). *$P < .05$ vs unirradiated group within same strain, +$P < .01$ vs WT mice receiving TBI only in other TBI-treated groups, ‡$P < .05$ vs $mpl^{-/-}$ mice receiving TBI only in groups with specific receptor blockade (comparisons performed by 1-way ANOVA and Dunnett posttest analysis). (C) Immunostaining (20×) for BrdU incorporation (black) in CD41-expressing (red) megakaryocytes (arrowheads) in WT vs $mpl^{-/-}$ BM 48 hours after TBI. (D) At 48 hours post-TBI in WT BM (left), few BM cells remain, and none with the morphologic appearance of megakaryocytes display TUNEL$^+$ (brown stain, black arrow) apoptosis, compared with a ligase-treated positive control serial section (right), with megakaryocytes (arrowheads) present in each section (20×). (E) Total megakaryocyte number per HPF (20×) in the same groups as in (B). +$P < .01$ vs baseline WT or WT TBI-only group (comparisons performed by 1-way ANOVA and Dunnett posttest analysis).

surface (Figure 1A). At baseline, only 14% of marrow megakaryocytes resided proximal to the endosteum, compared with 43% post-TBI (Figure 1B; $P < .01$). To determine whether megakaryocyte relocation results from active migration or selective survival, we administered BrdU to mice at 24 and 42 hours post-TBI, observing BrdU incorporation in CD41$^+$ megakaryocytes at 48 hours post-TBI (Figure 1C). TUNEL assays demonstrated no apoptotic cells with the morphologic appearance of megakaryocytes 48 hours post-TBI (Figure 1D). Additionally, on histology measurements, the total BM megakaryocyte numbers in WT mice were not significantly reduced by TBI (Figure 1E; $P = .08$). Furthermore, the percentage of megakaryocytes as a fraction of the total live BM cells increased by 10-fold vs baseline in 48-hour post-TBI mice, demonstrating prolonged survival of megakaryocytes relative to other BM cell populations (supplemental Figure 1A-B). Together, these findings indicate that megakaryocyte localization to the endosteal niche post-TBI reflects dynamic migration of viable, metabolically active cells.

c-MPL–deficient ($mpl^{-/-}$) mice lacked TPO responsiveness and showed a 63% reduction in baseline BM megakaryocyte number relative to WT mice (Figure 1E), consistent with published findings.[23,24] At 48 hours post-TBI, $mpl^{-/-}$ mice had a 65%

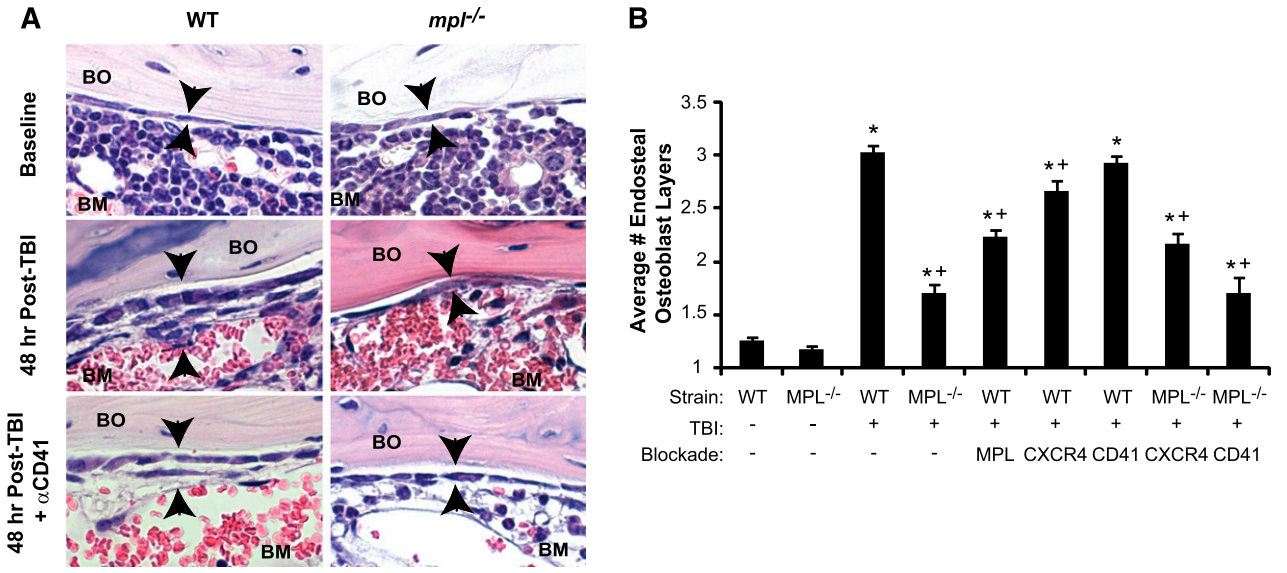

Figure 2. Blockade of TBI-induced c-MPL–dependent megakaryocyte endosteal migration abrogates niche osteoblast expansion post-TBI. (A) H&E sections (63×) of WT (left panels) and $mpl^{-/-}$ (right panels) metaphyseal bone (BO) and BM at baseline (top) and 48 hours post-TBI in the presence (bottom) or absence (middle) of CD41 blockade, demonstrating a single layer of endosteal osteoblasts at baseline followed by proliferation and expansion of endosteal osteoblasts in WT BM 48 hours post-TBI that is markedly attenuated by c-MPL deficiency, but not CD41 blockade. (B) Quantitative scoring analysis of osteoblast layer number (mean ± SEM) at baseline in WT and $mpl^{-/-}$ mice (n = 5 mice each); in WT mice receiving TBI only (n = 19), or blockade of c-MPL (n = 10), CXCR4, or CD41 (n = 5 each); and in $mpl^{-/-}$ mice receiving TBI only (n = 19) or TBI plus blockade of CXCR4 or CD41 (n = 5 each). *$P < .01$ vs unirradiated group within same strain, +$P < .05$ vs WT mice receiving TBI only in TBI-treated groups (comparisons performed by 1-way ANOVA and Dunnett posttest analysis).

reduction compared with WT mice, specifically in the percentage of megakaryocytes migrating to the endosteum ($P < .01$; Figure 1B). To determine whether this deficit reflected developmental abnormalities in $mpl^{-/-}$ megakaryocytes or, specifically, lack of TPO responsiveness, we treated WT mice after TBI with AMM2, a c-MPL–blocking antibody. AMM2 treatment did not decrease total megakaryocyte numbers post-TBI, (Figure 1E) but was associated with a 42% reduction in megakaryocyte endosteal migration (Figure 1B; $P < .01$ relative to WT), indicating a key role for TPO/c-MPL signaling in this pathway.

Functional blockade of megakaryocyte-expressed CXCR4[14] or $\alpha_{IIb}\beta_3$ integrin[25] in WT mice with AMD3100 or anti-CD41 (α_{IIb} subunit)–blocking antibody (MWREG30), respectively, also significantly reduced ($P < .01$, each comparison) megakaryocyte endosteal migration post-TBI (Figure 1A-B). Deficiency of c-MPL combined with CD41 blockade, but not with CXCR4 blockade, synergistically reduced endosteal megakaryocytes to baseline pre-TBI percentages (Figure 1B).

TPO-dependent megakaryocyte signaling is required for TBI-induced osteoblast expansion

In WT mice, TBI induced not only endosteal osteoblast expansion from a single layer at baseline to 3 to 4 layers, but also induced morphologic changes in individual osteoblasts from flattened to a cuboidal morphologic pattern (Figure 2A), which may increase adhesive interactions between the niche and HSC.[26] Megakaryocytes appeared to migrate specifically to sites of this endosteal osteoblast expansion (supplemental Figure 1C). Using a transgenic mouse model, we confirmed that the majority of this endosteal cell expansion is composed of mature osteoblasts (supplemental Figure 1D). In contrast, TBI-induced osteoblast expansion in $mpl^{-/-}$ mice was significantly diminished, with the endosteal surface lined by only 1 to 2 layers, and individual osteoblasts displaying baseline flattened morphologic features (Figure 2A). By quantitative scoring methods,[9] TBI-induced endosteal osteoblast expansion was reduced by 70% in $mpl^{-/-}$ vs WT mice (Figure 2B; $P < .001$).

Next, we examined osteoblast expansion in WT mice treated with AMM2 antibody to induce c-MPL blockade at the time of TBI, thereby excluding developmental effects of c-MPL deficiency, including decreased megakaryocyte numbers. This strategy resulted in decreased post-TBI osteoblast expansion compared with that in untreated WT mice (44% reduction; $P < .001$), although osteoblast expansion (1.9-fold; $P < .001$) exceeded that in post-TBI $mpl^{-/-}$ mice (Figure 2B). These findings suggest that both megakaryocyte c-MPL signaling and normal megakaryocyte numbers are necessary for maximal post-TBI endosteal niche remodeling, although we cannot exclude whether incomplete c-MPL blockade by AMM2 was responsible for the smaller decrease in osteoblast expansion produced by AMM2 treatment vs c-MPL deficiency.

CXCR4 antagonism in WT mice post-TBI led to a small but significant reduction (21%; $P < .05$) in osteoblast expansion (Figure 2B). Anti-CD41 treatment of WT or $mpl^{-/-}$ mice had no effect on post-TBI osteoblast expansion despite severely reducing megakaryocyte migration (Figure 2A-B). This finding led us to hypothesize that megakaryocyte-derived paracrine mediators dependent on c-MPL signaling, but not direct CD41 integrin-mediated megakaryocyte adhesion to the niche, may promote endosteal osteoblast expansion post-TBI.

PDGF-BB mediates megakaryocyte effects on osteoblast proliferation

To identify candidate paracrine mediators of TBI-induced endosteal osteoblast expansion, we examined BM osteoblast growth factor production at baseline vs 48 hours post-TBI, finding notable post-TBI increases in PDGF-BB (4.9-fold; $P < .001$), insulin-like growth factor (IGF)-1 (6.4-fold; $P < .001$), and VEGF (1.6-fold; $P < .02$)

(Figure 3A). Significant increases were also seen post-TBI in 2 megakaryocyte survival factors: SDF-1 and TPO (Figure 3A).

Supporting the candidacy of PDGF-BB, BM PDGF-BB levels at 48 hours post-TBI were decreased by 92% in $mpl^{-/-}$ vs WT mice (Figure 3B; $P < .001$). Although baseline PDGF-BB levels were also decreased in $mpl^{-/-}$ vs WT mice (supplemental Figure 2A), the specific increase in BM PDGF-BB after TBI was also reduced in $mpl^{-/-}$ vs WT mice (2.7- vs 4.9-fold; $P < .02$). In contrast, c-MPL blockade in WT mice produced only modest reductions in post-TBI levels of PDGF-BB ($P = .07$), suggesting that decreased BM megakaryocytes, rather than the absence of c-MPL signaling, causes decreased PDGF-BB production in $mpl^{-/-}$ BM. Similar to its effects on osteoblast proliferation, CD41 blockade in WT mice had no impact on PDGF-BB levels. In contrast to PDGF-BB, post-TBI BM levels of VEGF, IGF-1, and SDF-1 did not differ significantly among WT, $mpl^{-/-}$, anti-CD41–treated WT, or anti-c-MPL–treated WT mice, whereas post-TBI BM TPO levels were increased 1.8-fold in untreated WT mice vs other groups ($P < .01$; Figure 3B).

PDGF receptor β (PDGFRβ) is expressed at high levels by endosteal osteoblasts both at baseline and 48 hours post-TBI (supplemental Figure 2B-C). To determine whether megakaryocyte-derived PDGF-BB mediates megakaryocyte effects on osteoblast expansion, we used an in vitro coculture system[13] with isolated primary osteoblasts and purified ex vivo–expanded primary megakaryocytes (Figure 3C). After 5 days, osteoblasts cocultured with megakaryocytes demonstrated 2.2-fold increased growth relative to osteoblasts cultured alone ($P < .001$); reciprocally, coculture with osteoblasts led to enhanced growth and survival duration of the megakaryocyte fraction (Figure 3D). Osteoblasts cocultured with megakaryocytes produced significantly more IGF-1, VEGF, and SDF-1 than did cultures of osteoblasts alone, whereas megakaryocyte-derived PDGF-BB levels decreased when megakaryocytes were cocultured with osteoblasts, suggesting consumption of PDGF-BB by expanding osteoblasts (Figure 3E; $P < .001$). When cultured across a 0.4-μm transwell membrane, megakaryocytes still significantly increased osteoblast growth vs cultures of osteoblasts alone ($P < .005$) (Figure 3F), indicating again that megakaryocyte-derived paracrine factors drive osteoblast growth. Importantly, the addition of PDGF-BB to osteoblast cultures recapitulated the enhancement of osteoblast growth seen with megakaryocyte coculture (Figure 3G). Furthermore, treatment of megakaryocyte/osteoblast cocultures with imatinib, a potent inhibitor of PDGFR signaling,[27] completely abolished both megakaryocyte-induced osteoblast expansion and osteoblast effects on megakaryocyte survival in vitro (Figure 3D). By contrast, neither c-MPL nor CD41 inhibition blocked growth of cocultured megakaryocytes and osteoblasts (Figure 3D), consistent with the failure of these manipulations to inhibit BM PDGF-BB production in vivo (Figure 3B).

To determine whether PDGF-BB is also required for TBI-induced endosteal osteoblast expansion in vivo, we treated mice pre- and post-TBI with imatinib. Similar to inhibition seen in $mpl^{-/-}$ mice, blockade of PDGFR signaling induced by imatinib resulted in near-complete abrogation of endosteal osteoblast expansion post-TBI, and as a consequence of either blocking niche expansion or inhibiting megakaryocyte PDGFR signaling directly, post-TBI imatinib treatment led to decreased megakaryocyte endosteal migration (Figure 3H-I). We next treated both WT and $mpl^{-/-}$ mice after TBI with recombinant PDGF-BB, finding that PDGF-BB not only enhanced TBI-induced endosteal osteoblast expansion in WT mice but also partially rescued the niche osteoblast expansion deficit in $mpl^{-/-}$ mice (Figure 3J and supplemental Figure 2D). Thus, PDGF-BB is a critical megakaryocyte-derived mediator of niche osteoblast expansion after TBI.

Post-TBI megakaryocyte modulation of the endosteal niche is required for efficient donor progenitor and LT-HSC engraftment

As reported previously,[24] baseline long-term (LT)-HSC were reduced by 76% in $mpl^{-/-}$ vs WT BM, although $mpl^{-/-}$ BM compensates for this deficit, by producing relatively normal numbers of late hematopoietic progenitors, leading to overall normal BM cellularity at baseline (Figure 4A and supplemental Figure 3A-B). To assess whether diminished post-TBI megakaryocyte-driven endosteal osteoblast expansion in $mpl^{-/-}$ mice influences the efficiency and speed of initial donor BM engraftment and hematopoietic expansion, while avoiding confounding effects from decreased HSC in $mpl^{-/-}$ mice, we transplanted transgenic GFP^+ BM[20] with normal c-MPL expression into irradiated (48-hour post-TBI) WT or $mpl^{-/-}$ primary (1°) recipients. Because CD41 is not expressed on LT-HSC,[28] and anti-CD41 treatment of donor BM did not alter donor HSC engraftment in control studies (data not shown), we also asked whether blockade of host megakaryocyte migration post-TBI by anti-CD41 treatment alters donor GFP^+ BM engraftment.

From 24 hours through 3 weeks post-1° transplantation (Figure 4B-D), GFP^+ BM engraftment and expansion were significantly reduced ($P < .01$) by CD41 blockade (33%-49% reduction), c-MPL deficiency (40%-55%), or both (41%-65% reduction). HSC and progenitor cells were not detectable by flow cytometry using the established $c\text{-}Kit^+lin^-Sca\text{-}1^+$ (KLS) immunophenotype within the BM of primary recipients for the first 3 days after primary transplant (Figure 4E), even when $SCA\text{-}1^+$–selected BM was used as the donor BM source (supplemental Figure 3C-D), possibly because of either inadequate sensitivity of flow cytometry–based detection or temporary alteration of the surface immunophenotype of stem/progenitor populations posttransplant. However, at 5 and 7 days posttransplant, recovery of KLS cells occurred earlier and to a greater extent in WT vs anti-CD41–treated $mpl^{-/-}$ primary recipients (Figure 4E).

Next, we asked whether CD41 blockade or c-MPL deficiency inhibited the efficiency of initial engraftment and expansion specifically of ST or LT-HSC engraftment. To address this question, we conducted competitive secondary transplantation repopulation assays,[22] using GFP^+ donor BM as the donor source for 1° transplantation, and irradiated WT, $mpl^{-/-}$, or anti-CD41–treated WT mice as 1° recipients (Figure 5A). In these assays, secondary (2°) BMT was performed at either 24 hours or 3 weeks after 1° BMT to assess differences in homing/initial HSC engraftment only and combined initial engraftment and expansion, respectively. Harvested 1° recipient BM was transplanted at a 5% BME dose[22] (one fifth of all BM collected from one 1° recipient), together with unirradiated WT whole BM competitor cells into irradiated secondary (2°) recipient WT mice. Thus, the percentages of GFP^+ cells in 2° recipient peripheral blood lineages served as a read-out for relative HSC engraftment efficiency mediated by the distinct 1° recipient group niche microenvironments. When 2° BMT was performed 24 hours after 1° BMT, GFP^+ engraftment of RBC, platelet, total white blood count (WBC), $GR\text{-}1^+$ myeloid, and $B220^+$ lymphoid lineages at 3 weeks after 2° BMT, was decreased by 83%, 97%, 89%, >99%, and 68%, respectively ($P < .02$) in 2° recipients of $mpl^{-/-}$ vs WT 1° recipient BM (Figure 5B). The 1° recipient CD41 blockade also significantly reduced 2° recipient GFP^+ RBC (67%) and platelet (90%) reconstitution 3 weeks after 2° BMT. However, reconstitution of 2° recipients receiving even WT 1° recipient BM declined from 6 to 24 weeks after 2° BMT (supplemental Figure 4), suggesting that when 2° BMT is performed 24 hours after

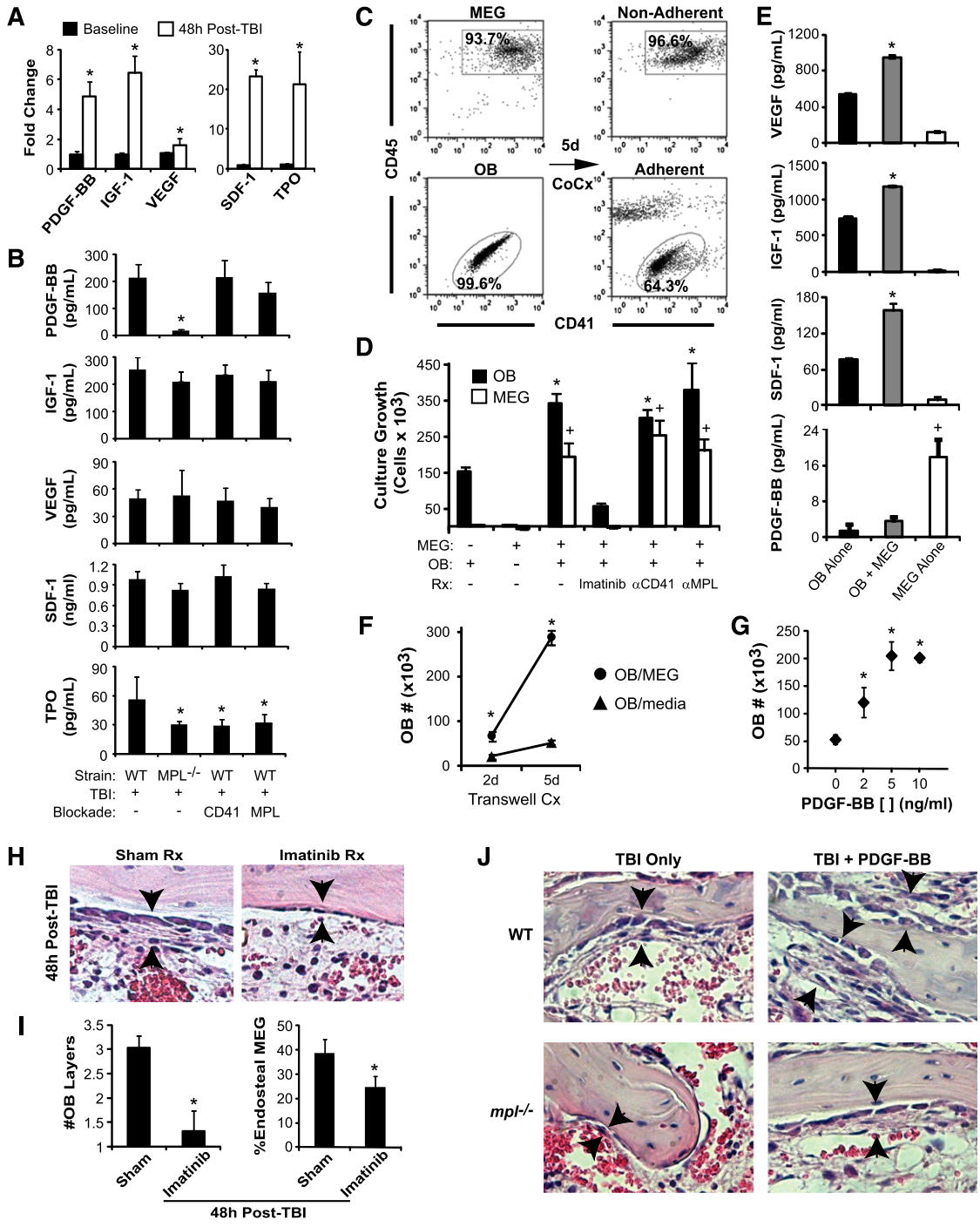

Figure 3. Megakaryocytes drive osteoblast expansion through PDGF-BB expression. (A) BM levels of PDGF-BB, IGF-1, VEGF, SDF-1, and TPO by ELISA (mean ± SD) at baseline and at 48 hours post-TBI in WT mice. *$P < .001$ vs baseline. (B) Levels of BM PDGF-BB, IGF-1, VEGF, SDF-1, and levels in WT vs *mpl*$^{-/-}$ mice with or without CD41 or c-MPL antibody blockade (n = 5 per group) at 48 hours post-TBI. *$P < .05$ vs WT TBI-only group. (C) Representative dot plots showing purity of isolated, ex vivo–expanded megakaryocytes (MEG) and primary osteoblasts (OB) before coculture (left), together with nonadherent (top right) MEG and adherent (bottom right) OB fractions after 5 days of coculture. (D) Five-day growth/survival of MEG and OB cultured separately or in combination (OB+MEG), with or without imatinib (5 μm), anti-CD41 antibody, or anti-c-MPL antibody (n = 3 each; mean ± SD). *$P < .01$ vs OB cultured alone, +$P < .001$ vs MEG cultured alone. (E) VEGF, IGF-1, SDF-1, and PDGF-BB supernatant concentrations (mean ± SD, n = 3 each) from 5-day cultures of OB, MEG, or cocultured OB + MEG. *$P < .001$ vs OB or MEG alone, +$P < .001$ vs OB alone or OB + MEG. (F) OB growth in 2- and 5-day OB cultures in which either MEG or medium alone was added to cultures across a 0.4-μM transwell membrane (n = 3 each). *$P < .002$ vs OB cultured with medium alone. (G) Five-day cultures of OB cultured with media alone or with increasing concentrations (2-10 ng/mL) of recombinant PDGF-BB (n = 3 each). *$P < .01$ vs cultures without PDGF-BB. (H) H&E-stained sections (40×) of BM at 48 hours post-TBI, demonstrating abrogation of OB expansion (arrowheads) caused by imatinib (right) vs sham (left) treatment. (I) Quantitative analysis of average OB layers (left) and percentage of endosteal MEG (right) at 48 hours post-TBI in imatinib vs sham-treated WT mice (n = 5 mice per group). *$P < .005$ vs sham-treated mice. (J) 40× photomicrographs of H&E-stained metaphyseal BM sections at 48 hours post-TBI in WT and *mpl*$^{-/-}$ mice demonstrating that treatment with PDGF-BB enhances 48-hour post-TBI endosteal OB proliferation (black arrows) in both WT and *mpl*$^{-/-}$ BM.

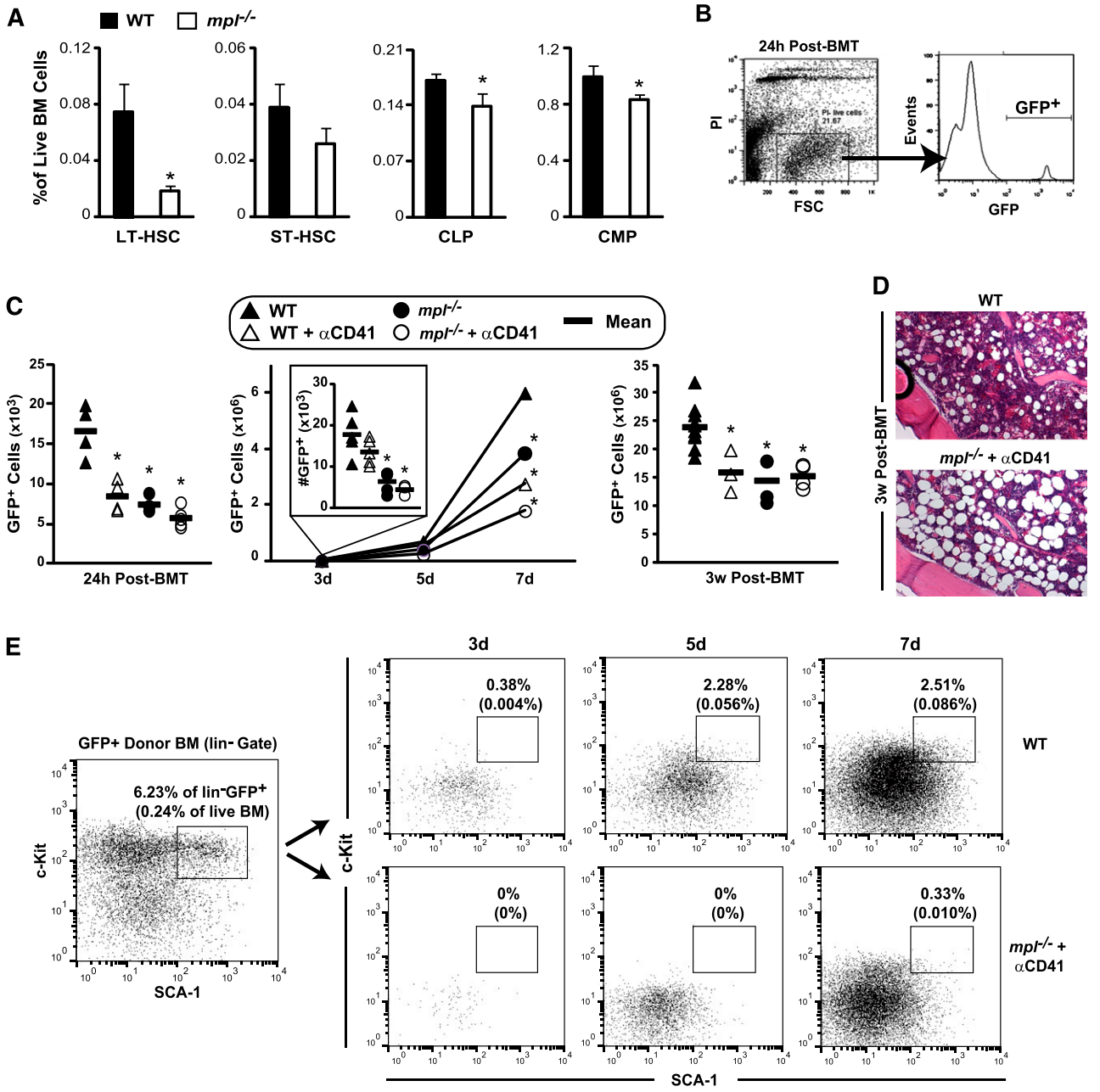

Figure 4. Blockade of host megakaryocyte function post-TBI decreases BM engraftment and expansion in primary transplant recipients. (A) Baseline LT-HSC (c-kit$^+$Lin$^-$SCA-1$^+$CD135^{lo}), ST-HSC (c-kit$^+$Lin$^-$SCA-1$^+$CD135$^+$CD34$^+$), common lymphoid progenitors (CLP, Lin$^-$CD127$^+$), and common myeloid progenitors (CMP, c-kit$^+$Lin$^-$SCA-1$^-$CD34$^+$CD127$^-$) in WT and *mpl*$^{-/-}$ BM, expressed as the percentage of all live BM cells (mean ± SD, n = 3 each). *$P < .05$ vs percentage in WT mice. (B) Representative dot plot and histogram demonstrating method of determining percentages of live, GFP$^+$ donor cells within irradiated recipient BM at 24 hours after BMT, used with total BM cell counts to determine absolute donor GFP$^+$ BM cells. (C) Absolute live BM GFP$^+$ donor cells (individual mice and/or mean per group) shown at 24 hours (left), 3 to 7 days (middle), and 3 weeks (right) post-BMT of 5 × 10^6 (24 hours to 7 days), or 2 × 10^5 (3 weeks) GFP$^+$ whole BM cells into post-TBI primary recipient WT or *mpl*$^{-/-}$ mice ± recipient treatment with anti-CD41 at the time of TBI (n = 3-5 mice per group). *$P < .05$ vs WT recipients. (D) H&E-stained histologic sections showing decreased BM cellularity in anti-CD41–treated *mpl*$^{-/-}$ (bottom) vs WT (top) recipients of GFP$^+$ donor BM at 3 weeks post-BMT. (E) Flow cytometry dot plots of c-Kit vs SCA-1 expression on live GFP$^+$Lin$^-$ gated whole BM cells from H2K-GFP donor BM before transplant (used to establish the HSC/progenitor c-Kit$^+$lin$^-$Sca-1$^+$ [KLS] gate), and from either WT (top, right) or anti-CD41–treated *mpl*$^{-/-}$ (bottom, right) primary recipients (pooled BM from 2-4 mice per time point), at 3, 5, and 7 days post-BMT with GFP$^+$ whole BM cells (3-5 × 10^6 cells per mouse). Rectangle in each plot represents KLS population with frequency expressed as a percentage of live GFP$^+$Lin$^-$ cells and of total live cells (in parentheses).

1° BMT, most measureable 2° recipient GFP$^+$ engraftment was the result of ST-HSC and primitive progenitor cells, but not LT-HSC.

We then performed 2° BMT 3 weeks after 1° BMT to assess for differences in both initial engraftment and early expansion of HSC caused by the distinct niche environments in our 1° recipient groups. Most 2° recipients of WT 1° recipient BM (57%) demonstrated multilineage GFP$^+$ reconstitution from 12 (Figure 5C) to 24 weeks (Figure 5D) after 2° BMT. Strikingly, c-MPL deficiency and CD41 blockade in the 1° recipient host megakaryocyte/endosteal niche produced ≥99% reduction in GFP$^+$ myeloid (GR-1$^+$), RBC, and platelet engraftment in 2° recipients at 12 weeks after 2° BMT (Figure 5C; $P < .001$), with smaller albeit significant reductions

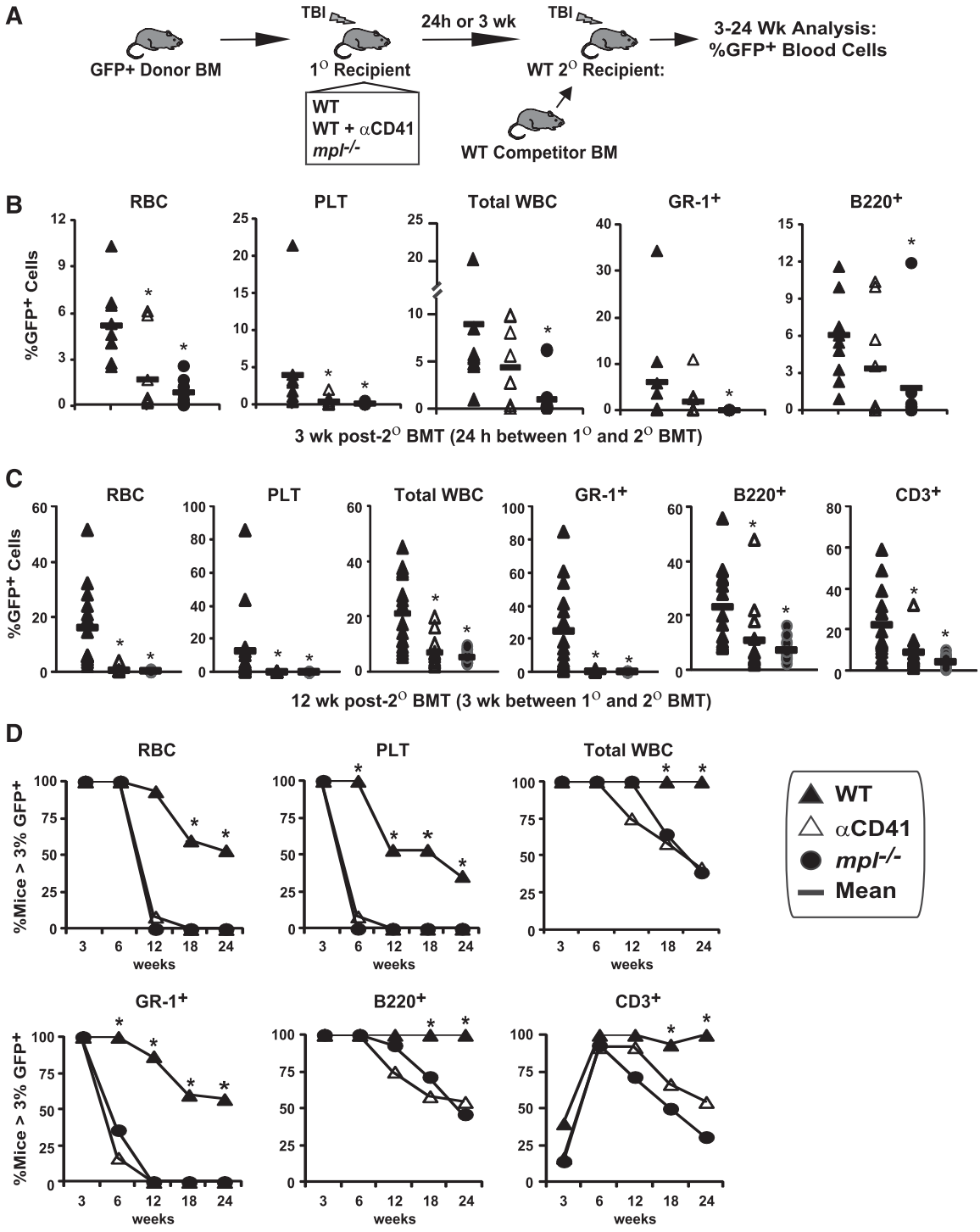

Figure 5. LT-HSC engraftment after BMT is severely impaired by blockade of host megakaryocytes. (A) GFP$^+$ donor engraftment in competitive secondary (2°) transplant (BMT) assays in which GFP$^+$ donor BM was transplanted (5×10^6 BM cells) into post-TBI WT, anti-CD41–treated WT, and *mpl*$^{-/-}$ primary (1°) recipients. (B) In the initial assay, BM was harvested 24 hours after 1° BMT and transplanted with 2×10^5 WT competitor BM cells into post-TBI WT 2° recipients. GFP$^+$ peripheral RBC, platelet, total WBC, myeloid (GR-1$^+$), and B-cell (B220$^+$) engraftment at 3 weeks after 2° BMT is shown. *$P < .05$ vs 2° recipients receiving WT 1° recipient BM. (C) Separate competitive transplant assay showing GFP$^+$ peripheral RBC, platelet, total WBC, myeloid, B-cell, and T-cell (CD3$^+$) engraftment at 12 weeks after competitive 2° BMT with 10^5 WT competitor BM cells, and either WT, WT + αCD41, or *mpl*$^{-/-}$ 1° recipient BM, harvested 3 weeks after 1° recipient BMT with 2×10^5 GFP$^+$ donor BM cells. *$P < .05$ vs 2° recipients receiving WT 1° recipient cells. (D) Percentage of competitively transplanted 2° recipients receiving WT, WT + αCD41, or *mpl*$^{-/-}$ 1° recipients cells 3 weeks after 1° BMT demonstrating >3% GFP$^+$ cells in specified lineage from 3 to 24 weeks after 2° BMT. *$P < .05$ vs percentage of 2° recipients of anti-CD41–treated or *mpl*$^{-/-}$ 1° recipient BM.

in lymphocyte engraftment ($P < .05$). These LT-HSC engraftment deficits remained significant through 24 weeks after 2° BMT (Figure 5D). We concluded that not only is TBI-induced niche osteoblast expansion required for efficient donor HSC engraftment, but megakaryocyte migration to the niche is also critical as CD41 blockade, which prevents megakaryocyte migration but not niche osteoblast expansion, severely impedes donor HSC engraftment.

TPO treatment enhances TBI-induced niche osteoblast expansion and engraftment after BMT

Having demonstrated that blockade of host megakaryocytes post-TBI impedes HSC engraftment, we hypothesized that augmentation of megakaryocyte function through TPO administration might enhance engraftment. Therefore, we administered TPO at low (10-μg/kg) and high (50-μg/kg) doses for 7 days before BMT using a schedule (Figure 6A), based on the half-life of TPO,[29] designed to limit treatment effects to the recipient's BM microenvironment pretransplant, thereby avoiding direct TPO effects on c-MPL–expressing donor HSC. Indeed, TPO levels in plasma or BM were not increased by the time of BMT in TPO- vs sham-treated mice using this schedule (supplemental Figure 5B).

TPO administered in the absence of TBI increased total numbers of BM megakaryocytes but did not induce significant endosteal osteoblast expansion (supplemental Figure 5A). Although low-dose TPO had only marginal effects, high-dose TPO given before TBI led to substantially increased endosteal megakaryocytes 48 hours post-TBI (Figure 6B). The increased megakaryocytes correlated with a 34% increase ($P < .001$) in osteoblast layer expansion at 48 hours post-TBI in high-dose TPO- vs sham-treated mice, with additional qualitative increases in osteoblasts displaying cuboidal (less flattened) morphologic patterns (Figure 6C-D). This increased endosteal osteoblast expansion was not associated with increased BM SDF-1 or PDGF-BB expression in high-dose TPO-treated mice (supplemental Figure 5C-D).

Primary transplant studies showed that high-dose TPO vs sham treatment of recipients led to a ~40% increase in GFP^+ donor BM engraftment 24 hours post-BMT (Figure 6E; $P < .05$). To test effects of TPO given before transplant on HSC engraftment, we performed another competitive secondary transplantation assay, selecting cell doses and timing between 1° and 2° transplants (36 hours) similar to the experiment in Figure 5B, where few 2° recipients of WT 1° recipient BM maintained GFP^+ LT-HSC engraftment. At 6 weeks after 2° BMT (Figure 6F), high-dose TPO treatment of 1° recipients before 1° BMT with GFP^+ donor BM led to increased mean percentages of 2° recipient GFP^+ RBC (3.9-fold; $P < .001$), myeloid $Gr\text{-}1^+$ cells (20-fold; $P < .02$), $B220^+$ B cells (14-fold; $P < .001$), and $CD3^+$ T cells (10-fold; $P < .02$) vs percentages in 2° recipients of sham-treated WT 1° recipient BM. At 28 weeks after 2° BMT, combined multilineage (myeloid, B cell, T cell) and progenitor (lineage-negative) GFP^+ BM engraftment, indicative of LT-HSC engraftment, was seen in 7 of 15 (47%) 2° recipients of high- dose TPO-treated 1° recipient BM vs only 1/14 (7%) 2° recipients of sham-treated 1° recipient BM (Figure 6G-H; $P < .05$), indicating that high-dose TPO administration pretransplant, with consequent enhanced megakaryocyte-driven niche remodeling, improves LT-HSC engraftment.

Discussion

Our data indicate that host megakaryocytes are recruited to the endosteal HSC niche after radioablative conditioning, where they stimulate niche expansion, and facilitate engraftment of HSC after transplantation. These conclusions are based on evidence that (1) decreased numbers of megakaryocytes, suppression of TPO/c-MPL signaling, and blockade of megakaryocyte-derived PDGF-BB signaling all abrogated TBI-induced niche osteoblast expansion; and (2) blockade of megakaryocyte recruitment to the niche prevented efficient engraftment of donor HSC after transplantation. Critically, we also show that megakaryocyte function can be augmented by TPO administered before transplantation, leading to enhanced LT-HSC engraftment.

A fundamental question in our studies using $mpl^{-/-}$ mice and c-MPL blockade was whether TPO signaling through c-MPL on megakaryocytes is a critical driver of post-TBI niche osteoblast expansion. Figure 1 and 2 support essential contributions from TPO/c-MPL signaling specifically on megakaryocytes but do not rule out roles for quiescent HSC, which also express c-MPL.[15] However, given that osteoblastic expansion occurs post-TBI, and TBI rapidly induces host HSC death, it is unlikely that c-MPL on HSC is a competing factor with megakaryocyte-derived signaling in regulating TBI-induced osteoblast expansion.

Megakaryocytes are the major source of BM PDGF-BB[30] at baseline, and the profound deficit in PDGF-BB levels post-TBI that we found in $mpl^{-/-}$ vs WT mice demonstrates that megakaryocytes are the principal source of BM PDGF-BB post-TBI as well. TPO signaling directly regulates megakaryocyte PDGF-BB expression[31]; thus, reduced PDGF-BB expression in $mpl^{-/-}$ mice post-TBI may result from both decreased total megakaryocytes and absent TPO signaling. Our data demonstrate that inhibiting or enhancing megakaryocyte function and PDGFR signaling, respectively, diminishes and increases both in vitro osteoblast growth as well in vivo post-TBI endosteal osteoblast expansion and suggest that megakaryocytes and their production of PDGF-BB appear to be both necessary and sufficient to enable post-TBI endosteal niche expansion.

Our finding that $mpl^{-/-}$ mice used as recipients in primary and secondary transplant assays display decreased hematopoietic reconstitution and HSC engraftment and expansion reflects defective niche function post-TBI caused by decreased megakaryocyte function, and is not confounded by absent c-Mpl expression on HSC in $mpl^{-/-}$ mice. Since the donor BM cells used in these assays had normal WT levels of c-MPL expression. It is possible that at longer time points than we have studied after primary transplant, recovery of donor BM cellularity in $mpl^{-/-}$ primary recipients would approach that seen in WT primary recipients, as niche defects may be corrected with time by donor megakaryocytes with normal c-MPL function. Thus, $mpl^{-/-}$ mice may not be an ideal model for studying effects of disrupting megakaryocyte/niche interactions on long-term durability of HSC engraftment in primary recipients. However, given that the primary goal of our transplant studies was studying the initial speed and efficiency of HSC engraftment short term (≤3 weeks) in primary recipients, it is unlikely that our results were significantly influenced by donor megakaryocyte effects on the niche.

An unexpected finding was that inhibition of the megakaryocyte-specific $\alpha_{IIb}\beta_3$ integrin via CD41 blockade severely impeded both megakaryocyte migration to the endosteal niche and HSC engraftment after transplantation, but did not significantly disrupt megakaryocyte-driven niche osteoblast expansion. $\alpha_{IIb}\beta_3$ integrin regulates homeostatic megakaryocyte migration through its binding to BM extracellular matrix components[32]; thus, abrogation of megakaryocyte migration post-TBI by anti-CD41 treatment is consistent with integrin-mediated adhesion blockade. As discussed above, anti-CD41 treatment of WT mice does not disrupt niche osteoblast expansion likely because it does not decrease the total megakaryocyte number or PDGF-BB expression. Importantly, abrogation of HSC engraftment by CD41 blockade suggests that the specific presence of megakaryocytes at the niche could also be necessary for maximal HSC engraftment efficiency. This hypothesis requires future confirmatory studies but is intriguing given the overlapping

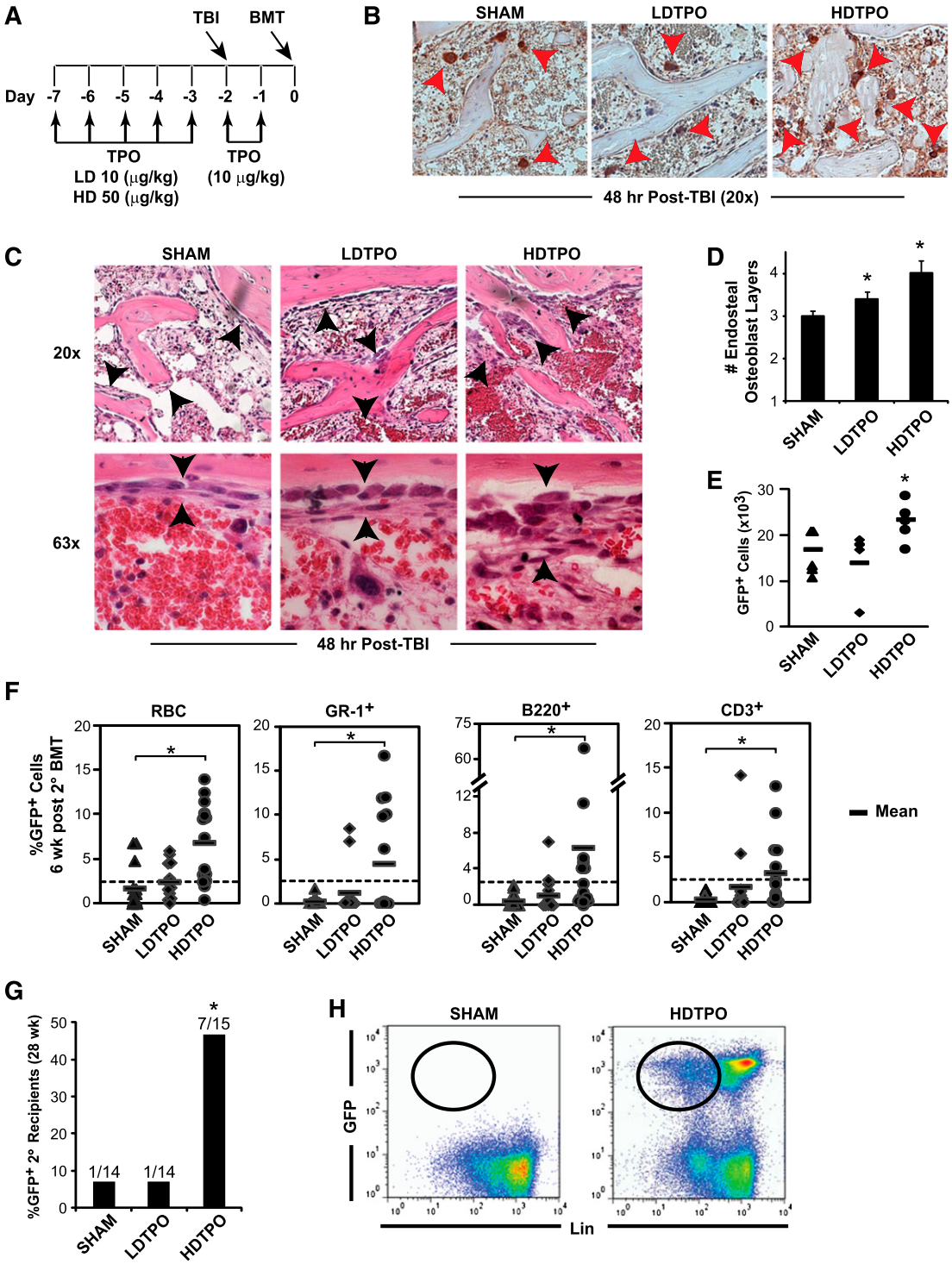

Figure 6. TPO administration before BMT enhances megakaryocyte-mediated expansion of niche osteoblasts and HSC engraftment. (A) Schedule of TPO administration. (B) Immunostained (CD41) sections (20×) comparing 48-hour post-TBI BM endosteal megakaryocytes (red arrowheads) after high-dose TPO (HDTPO, 50 μg/kg), low-dose TPO (LDTPO, 10 μg/kg), or sham treatment. (C) BM sections (20× top, 63× bottom) at 48 hours post-TBI showing increased endosteal osteoblast expansion (black arrowheads) after HDTPO treatment vs LDTPO- or sham-treated mice. (D) Quantitative assessment of 48-hour post-TBI osteoblast layers (mean ± SD) in sham-, LDTPO-, and HDTPO-treated WT mice (n ≥5 mice per group). *$P < .005$ vs sham-treated group. (E) Absolute BM GFP$^+$ engraftment at 24 hours post-BMT (5×10^6 cells) in post-TBI 1° recipients receiving sham, LDTPO, or HDTPO treatment (n = 5 per group). *$P < .05$ vs sham-treated group. (F) Secondary (2°) recipient GFP$^+$ peripheral RBC, myeloid (GR-1$^+$), B-cell (B220$^+$), and T-cell (CD3$^+$) engraftment at 6 weeks after 2° BMT with 2×10^5 WT competitor BM cells and either sham-, LDTPO-, or HDTPO-treated primary (1°) recipient BM at 24 hours after 1° recipient BMT. *$P < .02$ vs 2° recipients of sham-treated 1° recipient BM. (G) Percentage of 2° recipients of sham, LDTPO, or HDTPO 1° recipient BM with GFP$^+$ BM engraftment (>0.25% each) in myeloid, B-cell, T-cell, and Lin$^-$ BM populations at 28 weeks after 2° BMT. *$P < .05$ vs 2° recipients of sham-treated 1° recipient BM. (H) Representative dot plots of GFP vs Lin in BM at 28 weeks after 2° BMT in recipients of sham- vs HDTPO-treated 1° recipient BM.

functions of endosteal osteoblasts in both megakaryocyte and HSC development and homeostasis.[11,33]

Many strategies have been devised to address problems of inefficient engraftment and graft failure in clinical HSCT, although most efforts have focused on enhancing donor HSC function.[34] TPO has been administered after transplantation in clinical trials, but this strategy failed to either accelerate hematopoietic recovery or improve outcome.[35] By contrast, our TPO administration schedule, which led to significantly enhanced HSC engraftment, was chosen specifically to (1) increase resident megakaryocyte numbers before TBI; (2) increase TPO/c-MPL–dependent functions between TBI and transplantation; and (3) avoid direct effects of TPO on c-MPL–expressing donor HSC after transplantation. The precise cellular and molecular pathways by which TPO administration and consequent increased megakaryocyte function enhance HSC engraftment will require considerable future investigation. Regardless, clinical strategies using TPO mimetic treatment schedules that enhance megakaryocyte-driven HSC niche functions in recipients before transplantation may provide a novel approach to improving clinical transplantation engraftment outcomes.

Acknowledgments

The authors acknowledge Dr Alan Flake for provision of flow cytometry resources, Dr Masahiro Iwamoto for provision of histology equipment, and Drs Mortimer Poncz and Michele Lambert for technical expertise with megakaryocyte assays. The authors also acknowledge Genentech for providing founder mice for the $mpl^{-/-}$ colony and Kyowa Hakko Kirin for providing the AMM2 antibody. The authors thank John Gilbert for reviewing this manuscript.

This study was funded in part by the following research institutions: National Institutes of Health R01 HL077643 (E.M.H.), T32HL007150-34 (T.S.O.), the Fondazione Cassa di Risparmio di Modena (M.D., A.C.), Italian Ministry of Health, Bando Cellule Staminali e Malattie Rare 2008 (M.D.). The Canuso Foundation Innovation Grant (T.S.O., E.M.H.), and The 2011 American Society of Hematology Research Training Award for Fellows (T.S.O.).

Authorship

Contribution: T.S.O. participated in the design of all experiments, performed all experiments, analyzed and interpreted the data, and prepared the manuscript; A.C. participated in the experimental design and assisted with the ELISA and histology experiments; S.O. and T.J.H. helped design the experiments, assisted with transplantation and cell culture experiments, and assisted with data interpretation and review of the manuscript; R.W. discussed the hypothesis and conceived the idea of experiments involving PDGFR blockade; P.P. participated in the study design and review of the manuscript; M.D. conceived the initial hypothesis, helped design the experiments, and assisted with data interpretation and manuscript review; and E.M.H. oversaw the entire project, designed and analyzed the experiments, and participated in manuscript preparation.

Conflict-of-interest disclosure: The authors declare no competing financial interests.

The current affiliation for R.W. is Puma Biotechnology, Los Angeles, CA.

Correspondence: Edwin M. Horwitz, The Children's Hospital of Philadelphia, Colket Translation Research Building #3010, 3501 Civic Center Blvd, Philadelphia, PA 19104; e-mail: horwitze@e-mail.chop.edu.

References

1. Escalón MP, Komanduri KV. Cord blood transplantation: evolving strategies to improve engraftment and immune reconstitution. *Curr Opin Oncol.* 2010;22(2):122-129.
2. de la Morena MT, Gatti RA. A history of bone marrow transplantation. *Immunol Allergy Clin North Am.* 2010;30(1):1-15.
3. Garrett RW, Emerson SG. Bone and blood vessels: the hard and the soft of hematopoietic stem cell niches. *Cell Stem Cell.* 2009;4(6):503-506.
4. Zhang J, Niu C, Ye L, et al. Identification of the haematopoietic stem cell niche and control of the niche size. *Nature.* 2003;425(6960):836-841.
5. Xie Y, Yin T, Wiegraebe W, et al. Detection of functional haematopoietic stem cell niche using real-time imaging. *Nature.* 2009;457(7225):97-101.
6. Lo Celso C, Fleming HE, Wu JW, et al. Live-animal tracking of individual haematopoietic stem/progenitor cells in their niche. *Nature.* 2009;457(7225):92-96.
7. Castillo AB, Jacobs CR. Mesenchymal stem cell mechanobiology. *Curr Osteoporos Rep.* 2010;8(2):98-104.
8. Winkler IG, Sims NA, Pettit AR, et al. Bone marrow macrophages maintain hematopoietic stem cell (HSC) niches and their depletion mobilizes HSCs. *Blood.* 2010;116(23):4815-4828.
9. Dominici M, Rasini V, Bussolari R, et al. Restoration and reversible expansion of the osteoblastic hematopoietic stem cell niche after marrow radioablation. *Blood.* 2009;114(11):2333-2343.
10. Pallotta I, Lovett M, Rice W, Kaplan DL, Balduini A. Bone marrow osteoblastic niche: a new model to study physiological regulation of megakaryopoiesis. *PLoS ONE.* 2009;4(12):e8359.
11. Kacena MA, Gundberg CM, Horowitz MC. A reciprocal regulatory interaction between megakaryocytes, bone cells, and hematopoietic stem cells. *Bone.* 2006;39(5):978-984.
12. Kacena MA, Shivdasani RA, Wilson K, et al. Megakaryocyte-osteoblast interaction revealed in mice deficient in transcription factors GATA-1 and NF-E2. *J Bone Miner Res.* 2004;19(4):652-660.
13. Ciovacco WA, Cheng YH, Horowitz MC, Kacena MA. Immature and mature megakaryocytes enhance osteoblast proliferation and inhibit osteoclast formation. *J Cell Biochem.* 2010;109(4):774-781.
14. Zheng C, Yang R, Han Z, Zhou B, Liang L, Lu M. TPO-independent megakaryocytopoiesis. *Crit Rev Oncol Hematol.* 2008;65(3):212-222.
15. Yoshihara H, Arai F, Hosokawa K, et al. Thrombopoietin/MPL signaling regulates hematopoietic stem cell quiescence and interaction with the osteoblastic niche. *Cell Stem Cell.* 2007;1(6):685-697.
16. Lataillade JJ, Clay D, Bourin P, et al. Stromal cell-derived factor 1 regulates primitive hematopoiesis by suppressing apoptosis and by promoting G(0)/G(1) transition in CD34(+) cells: evidence for an autocrine/paracrine mechanism. *Blood.* 2002;99(4):1117-1129.
17. Zhao M, Ross JT, Itkin T, et al. FGF signaling facilitates postinjury recovery of mouse hematopoietic system. *Blood.* 2012;120(9):1831-1842.
18. Itkin T, Ludin A, Gradus B, et al. FGF-2 expands murine hematopoietic stem and progenitor cells via proliferation of stromal cells, c-Kit activation, and CXCL12 down-regulation. *Blood.* 2012;120(9):1843-1855.
19. Tanum G. The megakaryocyte DNA content and platelet formation after the sublethal whole body irradiation of rats. *Blood.* 1984;63(4):917-920.
20. Dominici M, Tadjali M, Kepes S, et al. Transgenic mice with pancellular enhanced green fluorescent protein expression in primitive hematopoietic cells and all blood cell progeny. *Genesis.* 2005;42(1):17-22.
21. Miccio A, Wang Y, Hong W, et al. NuRD mediates activating and repressive functions of GATA-1 and FOG-1 during blood development. *EMBO J.* 2010;29(2):442-456.
22. Szilvassy SJ, Ragland PL, Miller CL, Eaves CJ. The marrow homing efficiency of murine hematopoietic stem cells remains constant during ontogeny. *Exp Hematol.* 2003;31(4):331-338.
23. Majka M, Janowska-Wieczorek A, Ratajczak J, et al. Stromal-derived factor 1 and thrombopoietin regulate distinct aspects of human megakaryopoiesis. *Blood.* 2000;96(13):4142-4151.

24. Murone M, Carpenter DA, de Sauvage FJ. Hematopoietic deficiencies in c-mpl and TPO knockout mice. *Stem Cells.* 1998;16(1):1-6.

25. Teeling JL, Jansen-Hendriks T, Kuijpers TW, et al. Therapeutic efficacy of intravenous immunoglobulin preparations depends on the immunoglobulin G dimers: studies in experimental immune thrombocytopenia. *Blood.* 2001;98(4): 1095-1099.

26. Lee-Thedieck C, Rauch N, Fiammengo R, Klein G, Spatz JP. Impact of substrate elasticity on human hematopoietic stem and progenitor cell adhesion and motility. *J Cell Sci.* 2012;125(Pt 16): 3765-3775.

27. George D. Platelet-derived growth factor receptors: a therapeutic target in solid tumors. *Semin Oncol.* 2001;28(5 Suppl 17):27-33.

28. Kiel MJ, Yilmaz OH, Iwashita T, Yilmaz OH, Terhorst C, Morrison SJ. SLAM family receptors distinguish hematopoietic stem and progenitor cells and reveal endothelial niches for stem cells. *Cell.* 2005;121(7):1109-1121.

29. Kuter DJ. Thrombopoietin and thrombopoietin mimetics in the treatment of thrombocytopenia. *Annu Rev Med.* 2009;60:193-206.

30. Yoon SY, Tefferi A, Li CY. Cellular distribution of platelet-derived growth factor, transforming growth factor-beta, basic fibroblast growth factor, and their receptors in normal bone marrow. *Acta Haematol.* 2000;104(4):151-157.

31. Shimoda HK, Yamamoto M, Shide K, et al. Chronic thrombopoietin overexpression induces mesangioproliferative glomerulopathy in mice. *Am J Hematol.* 2007;82(9):802-806.

32. Mazharian A, Thomas SG, Dhanjal TS, Buckley CD, Watson SP. Critical role of Src-Syk-PLCgamma2 signaling in megakaryocyte migration and thrombopoiesis. *Blood.* 2010; 116(5):793-800.

33. Kidd S, Bueso-Ramos C, Jagan S, et al. In vivo expansion of the megakaryocyte progenitor cell population in adult CD26-deficient mice. *Exp Hematol.* 2011;39(5):580-590.e1.

34. Rocha V, Broxmeyer HE. New approaches for improving engraftment after cord blood transplantation. *Biol Blood Marrow Transplant.* 2010;16(1 Suppl):S126-S132.

35. Kuter DJ, Begley CG. Recombinant human thrombopoietin: basic biology and evaluation of clinical studies. *Blood.* 2002;100(10):3457-3469.